Available online at www.sciencedirect.com
ScienceDirect
Advances in Space Research 39 (2007) 590–604
ADVANCES IN SPACE RESEARCH (a COSPAR publication)
www.elsevier.com/locate/asr

The chemical composition of micrometeoroids impacting upon the solar arrays of the Hubble Space Telescope

A.T. Kearsley [a,*], G.A. Graham [b], J.A.M. McDonnell [c], E.A. Taylor [c], G. Drolshagen [d], R.J. Chater [e], D. McPhail [e], M.J. Burchell [f]

[a] Department of Mineralogy, The Natural History Museum, London, SW7 5BD, UK
[b] Institute of Geophysics and Planetary Physics, Lawrence Livermore National Laboratory, 7000 East Avenue, Livermore, CA 94550-9234, USA
[c] Planetary and Space Sciences Research Institute, The Open University, Milton Keynes, MK7 6AA, UK
[d] ESA/ESTEC, Noordwijk, The Netherlands
[e] Department of Materials Science, Imperial College of Science Technology and Medicine, London, SW7 2BP, UK
[f] Centre for Astrophysics and Planetary Sciences, School of Physical Science, University of Kent, Canterbury, Kent CT2 7NR, UK

Received 30 September 2004; received in revised form 13 May 2006; accepted 16 May 2006

Abstract

Analytical scanning electron microscopy of solar cells returned from the Hubble Space Telescope (HST) at the end of HST Service Missions SM-1 (1993) and SM-3B (2002) has revealed abundant remains of micrometeoroids. We have documented the most common residue compositions, and in this paper we suggest how they relate to mineral phases, and show how it is possible to estimate the proportion of the original micrometeoroid preserved. From a total of 273 impacts examined and analysed, we found 61/162 impacts on solar cells from SM-1 were produced by micrometeoroids, as were 45/111 from SM-3B. In each survey approximately 25% of damage features could not be assigned to a particular origin (micrometeoroid or space debris). A cumulative micrometeoroid flux curve for randomly selected cells shows impact features ranging from 3 to nearly 3800 μm in size. To assist interpretation of space exposed surfaces, impact residues from known meteoritic and terrestrial analogue mineral phases were produced by light gas gun assisted acceleration of buckshot projectiles into solar cell targets at 5.5–6.3 km s^{-1}.

Mg- and Fe-rich residues were found in 30/61 impacts from SM-1 and 26/45 from SM-3B, with variable Mg:Fe ratio, usually lacking Ca, and likely to be from olivine or low-Ca pyroxene. Only in a few examples is it possible to determine the divalent cation to silicon ratio, and thereby positively identify olivine or pyroxene. Vesicular Fe-, Mg-, Ni- and S-rich residues, found in eight impacts from SM-1 and 5 from SM-3B, closely resemble residue from light gas gun shots of phyllosilicate-rich meteorite grains, and may be from a layered silicate such as serpentine or smectite interlayered with tochilinite. Fe- and S-rich immiscible melt droplets, low in nickel, are probably of troilite origin. Fe-, Ni- and P-rich residue is almost certainly from the phosphide schreibersite, and iron–nickel metal residues show an elemental ratio characteristic of kamacite. One Mg-, Cr-, Fe- and O-rich residue suggests a spinel precursor. Ca-rich particles found within the spall zone of several craters closely resemble residue from calcium carbonate. Mg sulfates are also present. Very little aluminous silicate residue was found (one residue from each survey). One extraordinarily well-preserved assemblage contains residues from five mineral components and may represent impact by a chondrule fragment. Derivation of incident particle sizes from impact feature dimensions, by use of calibrated damage equations, reveals that the majority of impacting micrometeoroids had diameters of less than 10 μm, although the mass flux is concentrated in grains of more than 50 μm diameter. In one well-preserved crater, the mass of residue was calculated to be 60 ng, approximately 25% of the particle mass as suggested by experimental crater size calibration. The smallest impacts were produced by grains of between 600 nm and 1.3 μm. The most common residue assemblages suggest that the majority of micron to millimetre scale micrometeoroids have an origin from chondritic material, similar to interplanetary dust particles, micrometeorites, and possibly the hydrous carbonaceous chondrites of the CM, CR or CI group. The relative contribution of cometary as opposed to asteroidal particle sources cannot yet be assessed from this data set.

* Corresponding author.
E-mail addresses: antk@nhm.ac.uk (A.T. Kearsley), graham42@llnl.gov (G.A. Graham).

0273-1177/$30
doi:10.1016/j.asr.2006.05.011

Keywords: Micrometeoroid; Hypervelocity impact; Hubble Space Telescope; Analytical electron microscopy

1. Introduction

It is possible to obtain samples of extraterrestrial fine particles (cosmic dust) by a number of different methods, each of which imposes different limitations on interpretation of the composition and provenance of the collected particles. Due to the high relative velocity of most particles entering Earth's atmosphere, many undergo thermal and oxidative alteration and may be selectively melted (Alexander and Love, 2001), contaminated, or simply difficult to distinguish from abundant terrestrial dust. Nevertheless, pristine interplanetary dust particles (IDP) have been successfully captured by high altitude aircraft, and have yielded excellent structural and compositional information (Brownlee, 1985; Rietmeijer, 1998; Bradley, 2004). However, the limited numbers of particles captured during such collections do not easily permit measurement of the flux of particle masses and sizes. Micrometeorite collections made from bulk polar ice samples (Taylor et al., 1998) sample short time intervals (years) or integrated temporal flux for a relatively long time interval (centuries), but may themselves show compositional bias due to weathering. Ice collections also require very large sample sizes to reach the area–volume product of deep sea sediment samples, necessary for recognition of statistically significant numbers of the larger (>100 μm) particles, and sufficient for reliable measurement of extraterrestrial mass flux (Peucker-Ehrenbrink and Ravizza, 2000). Are there other collection methods that may yield substantial numbers of particles for examination, from known time intervals and without confusion with terrestrial contamination?

Two different approaches may be tried for deliberate collection of micrometeoroid particles in space: onboard analysis by sophisticated spectrometers (e.g. the Gorid detector, Svedhem et al., 1999); or use of dedicated capture media on spacecraft (e.g. low density silica aerogel, Hörz et al., 2000) followed by return to Earth for analysis. Returned samples can be subjected to an ever-increasing range of sophisticated laboratory instrumentation (Zolensky et al., 2000). However, in all these cases the area and time available for particle capture may be limited (an area-time product of a few m^2a at most), the total number of particles collected is likely to be small, and sampling of larger particles limited.

Opportunistic examination of impact residues on non-dedicated surfaces has also proven valuable (Graham et al., 2000, 2001b, 2002). In this present paper we show that hypervelocity impact residues on solar cells from the Hubble Space Telescope (HST) can reveal much about the size, composition, and even the origin, of micrometeoroids.

We have sought to answer the following questions: What are the most common micrometeoroid residue compositions and how do they relate to mineral phases that may have dominated the micrometeoroid particles? How big were the particles? What proportion of an original micrometeoroid particle has survived to be preserved within a crater? What are the origins of the micrometeoroids?

2. Samples, experimental and analytical parameters

The solar arrays removed from the HST during Service Mission 1 (SM-1) in 1993, and SM-3B in 2002, provided large numbers of particle impacts for analysis. In total, over 60 m^2 of array surface was returned by shuttle orbiters, the earlier SM-1 (single) array having been exposed to space in low Earth orbit (LEO) at an altitude of about 615 km for 3.6 years, and the two arrays from SM-3B at a similar altitude for 8.2 years. The survey methodology, areas sampled, and the results from impact feature counting and size measurement are described in McDonnell and Griffiths (1998) and Moussi et al. (2005), respectively. In addition to the major survey, individual solar cells (73 from SM-1 and 25 from SM-3B), each measuring 4 cm by 2 cm (Fig. 1), were cut from the arrays for more detailed impact feature imaging, measurement and analysis. Two types of investigation were then performed using analytical scanning electron microscopy: location and analysis of residue in selected larger impact features with diameter of conchoidal spallation (D_{co} of Herbert and McDonnell, 1997) greater than 100 μm; and full analytical characterisation of every impact feature greater than 3 μm D_{co} on a suite of randomly chosen solar cells (42 cells from SM-1 and 6 cells from SM-3B). The methodology for distinction of space debris and micrometeoroid residues has been described by Kearsley et al. (2005). The ratio of proven micrometeoroid and space debris impacts in defined size ranges was then used to select appropriate velocity regimes for application in the damage equations (as previously determined by Herbert et al. (2001)). On this basis, the numbers of micrometeoroid particles in defined size ranges

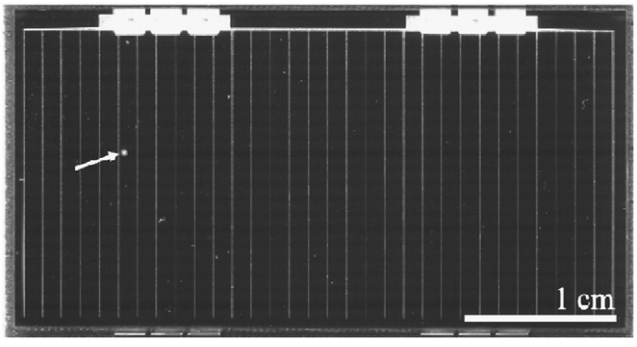

Fig. 1. Optical scan of a single solar cell returned from the Hubble Space Telescope by the SM-3B service mission. The large impact feature (arrowed) contains residue from a magnesium-rich silicate of micrometeoroid origin.

could be determined, and a flux curve generated (Moussi et al., 2005). The large numbers of very small individual particles, perhaps as small as 1 micron, provide information in a size range below the normal minimum recognised in terrestrial collections. Although the residue analyses presented in this paper were performed on samples with relatively low area- time product exposures (0.12 m^2a for SM-1, and 0.04 m^2 a for SM-3B), their impact fluxes and feature size distributions are very close to those determined from the larger surveys of Moussi et al., which were based upon very large area-time values (75 m^2 a for SM-1, and 340 m^2a for SM-3B for particles of between 120 and 300 μm diameter). These values represent the largest impact flux measurement campaigns on a single substrate that has ever been mounted in orbit and are between one and two orders of magnitude larger than the threshold (2.5 m^2a) for reliable statistical sampling of the mid range micrometeorite population (~150 μm) demonstrated by Peucker-Ehrenbrink and Ravizza, 2000. Although the mass flux is concentrated in the larger particles, the smaller grains (<20 μm) are present in much larger numbers (more than ten times, Moussi et al., 2005), and a reliable measurement of their numbers can therefore be made in a sample of smaller area-time product. As the attribution of micrometeoroid origin within our study is based upon residue analysis, we are also able to exclude a contribution from high eccentricity geostationary transfer orbit space debris (mainly solid rocket motor exhaust products, Hörz et al., 2002), thereby removing a flux component that was not recognised in the seminal work on the space-facing surface of the Long Duration Exposure Facility (Love and Brownlee, 1993). The fluxes presented by Moussi et al. (2005) should therefore be considered the most reliable for space environment modelling.

Solar cells were carbon-coated and examined using backscattered electron imagery (BEI) in Jeol 840, Jeol 5900LV and LEO 1455VP scanning electron microscopes, at 2 nA current and 20 kV accelerating voltage. X-ray analyses and maps were obtained using Oxford Instruments exL and INCA energy dispersive (ED) X-ray spectrometers. The imaging and analysis protocols are described at length in Graham et al. (2001a) and Kearsley et al. (2005), and have been extensively tested on impact features created in the laboratory (e.g. Graham et al., 1999). The laminate structure and composition of individual layers within HST solar cells is illustrated in Fig. 2. Most of the residues discussed in this paper are from impacts onto the 'top' sun-facing glass surface of the arrays, and were initially located by survey of the cell surface in secondary electron imaging mode. Impact features are much more difficult to find on the woven glass fibre behind the cell, and the range of interfering compositions in glass fibres and resin filler also make distinction of impactor chemistry problematic. Residues within impact features were located by X-ray mapping to reveal elemental enrichments that could not be explained by the cell composition, and ED spectra were obtained from areas rich in residue and from neighbouring uncontaminated substrate. The uniform composition of the borosilicate cover glass across the cell top surface, as determined in detail on a Cameca SX50 wavelength dispersive X-ray microprobe, also provided a comparable substrate for all the smaller impact features. In impact features of millimetre scale, residue may be found on deeper layers of the solar cell, including silicone resin and silicon. Residue mixing with the cover glass (rich in Si, Ce, Zn, K, Na and Al, with minor Mg, Ti and Ba) might be expected to make compositional determination difficult, but provided a wealth of spectral lines from which could be calculated approximate mixing ratios for solar cell glass and micrometeoroid components. The spectra of residue and substrate were overlain for comparison, and any enrichment in elements diagnostic of a micrometeoroid origin was noted (Fig. 3). The wide range of X-ray peak energies also allowed low concentrations of residue to be located even when topographic artefacts were dominant and absorption of low energy X-rays became substantial. Cross sections were sputter eroded in carefully selected locations using a 30 keV gallium ion beam in an FEI FIB200 TEM workstation to determine the depth of residue-bearing melt.

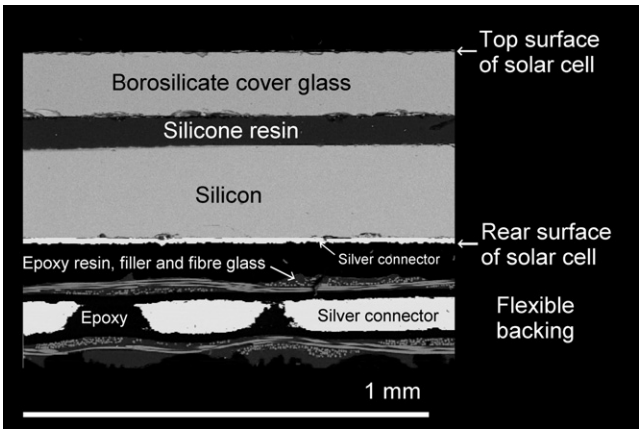

Fig. 2. Backscattered electron image showing a vertical cross section through a typical solar cell from the SM-1 service mission. Note the laminate structure with borosilicate glass top layer overlying a silicone resin layer and silver connectors.

Due to mixing with melted solar cell glass, and the complex surface shape of the impact features, it is not usually practical to determine precise elemental ratios within in-situ micrometeoroid residue. However, there are recurring elemental assemblages which closely resemble those seen in laboratory impacts of known mineral projectiles. Classification of the original impactor compositional components (the mineral content) required comparison with residues from impacts of known, well-characterised mineral species. Light gas gun impacts with buckshot firings at the University of Kent (Burchell et al., 1999) used mineral projectiles of selected grain size fractions between 4 and 250 μm diameter, at velocities between 5.5 and 6.3 km s^{-1}. Although the velocity attainable by laboratory impacts of suitable analogues cannot reach the regimes of many

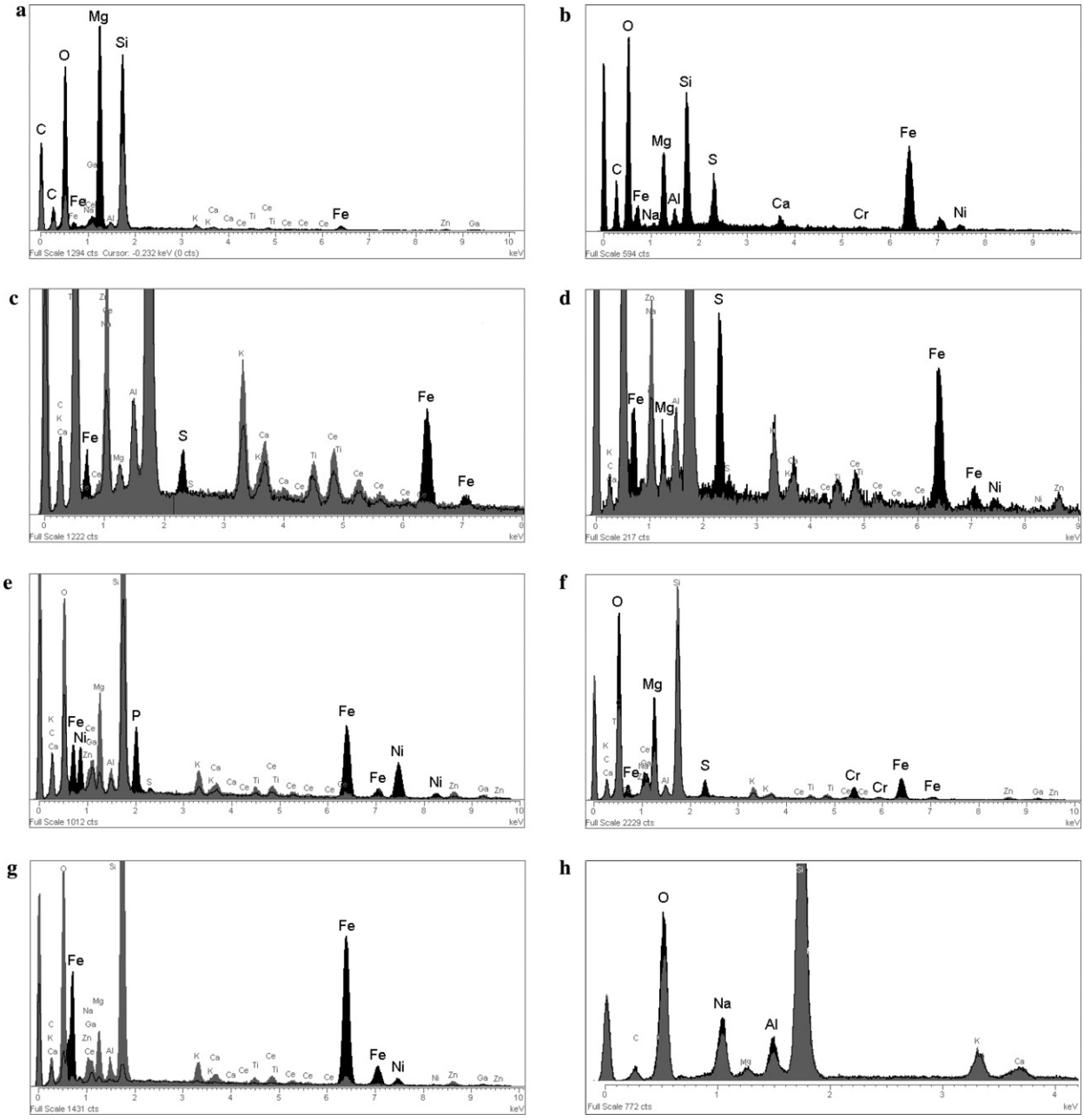

Fig. 3. (a) and (c)–(h) Representative ED X-ray spectra from micrometeoroid residues in craters on HST solar cells. In each case the spectrum from surrounding melted solar cell glass is shown in grey, with the residue spectrum superimposed in black: (a) Mg-rich residue from area giving olivine stoichiometry of Forsterite 98%; (b) see below; (c) Fe- and S-rich residue closely resembles troilite; (d) Fe-, Mg-, S- and Ni-rich residue probably from hydrous layer silicate (compare with (b); (e) Fe-, Ni- and P-rich residue with ratios close to those of schreibersite; (f)) Fe-, Cr-, Mg- rich residue intimately associated with Fe- and S-rich residue, probably chromite in troilite; (g) metallic Fe and Ni with peak ratios typical of kamacite; (h) Na-, Al-rich residue, probably either chondrule mesostasis glass or altered refractory inclusion silicate such as jadeite. Spectrum (b) shows the typical spectrum of the hydrous layered silicate phases found in the matrix and chondrule coatings of the CM-2 carbonaceous chondrite meteorite Murchison, compare this to spectrum (d).

natural micrometeoroids encountered in Earth orbit (40–70 km s^{-1}, Taylor, 1995), the morphology of impact features and chemical composition of residue from light gas gun shots do closely resemble those found on space exposed surfaces. Calculations based upon equations of state for silicate impactors and metallic targets (Bernhard et al., 1994) have shown that micrometeoroid impacts onto metal at 20 km s^{-1} should result in shock pressures in excess of 300 GPa, within the regime of melt and vapour generation from the projectile. Impacts onto the complex, but low density, solar cell surface may generate much lower pressures, with complete melting, but relatively little vapour generation. However, our laboratory impacts of materials rich in the volatile alkali metals sodium and

potassium onto solar cell glass do sometimes show depletion of these elements in the residue, suggesting their loss as vapour, as Hörz et al. (1983) found to occur during laboratory impacts onto aluminium. We have seen no evidence of substantial loss of other elements, including sulfur. Mixing and embedding of impactor with the borosilicate glass, followed by very rapid quenching, acts as a trap and prevents further alteration/loss, shown by the preservation of droplets of unoxidised metals (micrometeoroid iron–nickel and space debris aluminium) even where exposed to aggressive atomic oxygen in the low Earth orbit environment (Kearsley et al., 2005).

The selection of minerals for use as analogues was based upon those known to be dominant in collections of small particles such as Antarctic micrometeorites (Kurat et al., 1994), interplanetary dust particles (IDPs) collected in the stratosphere (Rietmeijer, 1998), and the more common minerals found in meteorites, especially those carbonaceous chondrite groups believed to be similar to common types of micrometeorites (Kurat et al., 1994). It is not practicable to use bulk examples of real micrometeorites or IDPs as projectiles for several reasons. The physical properties of many grains (e.g. cosmic spherules) may be unsuitable as analogues of pristine micrometeoroids because they have been subjected to high surface temperatures during atmospheric transit and now have compact internal structure and volatile element depletion. Our experience with shots of delicate projectiles (such as fine-grained phyllosilicates) suggests that the less altered aggregate IDPs would be too fragile to withstand the high acceleration generated within the gun, although they may have been relatively unharmed by exposure to space since their release from a parent body. Real analogues are also much too rare and valuable to use as projectiles, the necessary quantities for a single firing (many thousands of grains) might exceed the total mass picked during a campaign of ice/snow collection. We have used projectile powders from crushed carbonaceous chondrite meteorites Allende (CV3), Murchison (CM2) and Orgeuil (CI), but have found that the micron-scale mineral heterogeneity is so great that it prevents reliable identification as to the composition of many impacting particles, an essential constraint for their use as calibration materials. Consequently we have prepared grain-size sorted projectile powders from well-characterised and homogeneous coarse-grained samples of meteoritic and terrestrial minerals: olivine, enstatite, diopside, albite, anorthite, spinel, corundum, magnetite, pyrrhotite, kamacite, nepheline, serpentine group minerals and calcite (and many others). Samples of these projectiles can be obtained from the Natural History Museum for further work, and have now been used for diverse applications in laboratories worldwide.

3. Results and interpretation

In both post flight surveys, we were able to determine the type of impactor responsible for approximately 75% of the impact features examined. Distinction of the particle origins as debris or from micrometeoroids was explained in Kearsley et al., 2005. The smaller craters, less than 50 μm D_{co} were mainly of space debris origin (37 craters formed by micrometeoroids: 87 by space debris, mainly solid rocket motor combustion products). In contrast, most craters of greater than 50 μm diameter contained micrometeoroid residue (84 craters formed by micrometeoroids, 13 by space debris). The impact residue was of variable quantity and quality, dependant upon the preservation of the central melt pit (the frozen base of the transient crater). We found 61 small sub-circular or oval craters containing micrometeoroid residue during the SM-1 survey, and 45 during the SM-3B survey. The micrometeoroid impact residues found during the SM-3B survey are very similar in composition and abundance to those found in the solar cells from SM-1, except for the occurrence of a few, rarer residue types (Fig. 8). The cumulative flux curves in Figs. 9 and 10 are based upon all of the analysed craters from 3 μm to 4 mm on the random selection from SM-1 (42 cells) and SM-3B (6 cells), and are close to the values determined in the much larger survey of flux by Moussi et al. (2005). The logarithmic/logarithmic plots of Fig. 9 show the cumulative number of impact features created per square metre per second for the range of impact feature conchoidal glass detachment D_{co} sizes. The true total micrometeoroid flux may also include some particles that have left no distinguishable residue, and are thus hidden within the unresolved population (25% of SM-1 craters and 26% of SM-3B craters). The flux will thus exceed the confirmed 36% of SM-1 and 40% of SM-3B craters (dashed lines). To correct for this under-sampling, the micrometeoroid particle flux curves of Fig. 9 have been rescaled (the bold lines) by addition of a proportion of the unknown particle impacts, as determined from the ratio of proven space debris and micrometeoroid impacts in the appropriate size range. The rationale for determination of particle diameter from D_{co} as shown in Fig. 10 is discussed in Section 3.2 below.

The particle flux derived from the entire SM-3B survey funded by the European Space Agency and based upon optical imagery of many thousands of solar cells (340 m^2a area-time product), is described comprehensively in Moussi et al. (2005). Calibrated feature to particle size conversion equations (dependent upon determined particle origins and hence assumption of an appropriate velocity model) were employed by Moussi et al. (2005) to derive particle sizes based upon determined proportions of space debris and micrometeoroids, coupled with maximum and minimum flux limits from the number of features of unresolved origin.

3.1. Micrometeoroid residue compositions

Residue compositions are classified by those elements demonstrated to be present in excess over the substrate composition (Fig. 3).

3.1.1. Mg- and Fe-rich

Thin films enriched in Mg and Fe are the most common micrometeoroid residues found on HST cells, found in 30/61 impacts from SM-1 and 26/45 from SM-3B. The parent is likely to be olivine or low-Ca pyroxene, but an accurate divalent cation to silicon ratio cannot usually be determined due to dispersion in solar cell silicate glass melt (Fig. 3a). However, in some impacts there may be relatively large discrete patches of residue (Fig. 4), sufficiently flat to allow quantitative analysis by EDS. Calculation of the glass : impactor mixing ratio (based upon the known calcium, potassium, cerium and zinc contents of the solar cell glass, and their analysis in the glass-residue mix) reveals that the micrometeoroid component has an almost perfect stoichiometry for olivine of Forsterite 98%:Fayalite 2% composition. This is a widespread but relatively primitive composition, found throughout the IDP, micrometeorite and unequilibrated meteorite populations. Unfortunately, relatively few residues are sufficiently well-preserved to be identified to unequivocal mineral species as was possible in this case, and it is not possible to distinguish discrete compositional populations, as might aid comparison to other extraterrestrial materials (e.g. the olivine and pyroxene groups in Antarctic micrometeorites of Genge et al. (1997)). Mg- and Fe-rich residues are sometimes (4 craters) found associated with separate, discrete Fe- and S-rich or Fe–Ni metal residues, suggesting a polymineralic micrometeoroid impactor, with intimately intergrown grains of a few microns size.

3.1.2. Fe-, Mg-, Ni- and S-rich

These residues were found in nine features from SM-1 and 5 from SM-3B (e.g. Fig. 3d). They are usually vesicular, with gas bubbles appearing as dark patches in BE images. The association of elements resembles that seen in anhydrous IDPs (Bradley, 2004) although the textural evidence for presence of volatiles (probably water) may instead suggest an origin from hydrous layered phyllosilicates (serpentine or smectite) with interlayered Fe and Ni hydroxysulfide (tochilinite) in some examples. The Mg:Fe ratio differs between residues, possibly reflecting the variability reported by Rietmeijer (1998) for the Mg:Fe ratio in hydrous IDP components. Due to interference from the silicate substrate it is not possible to make a precise determination of the ratio of Mg plus Fe to Si, and hence which layer silicate mineral family is present.

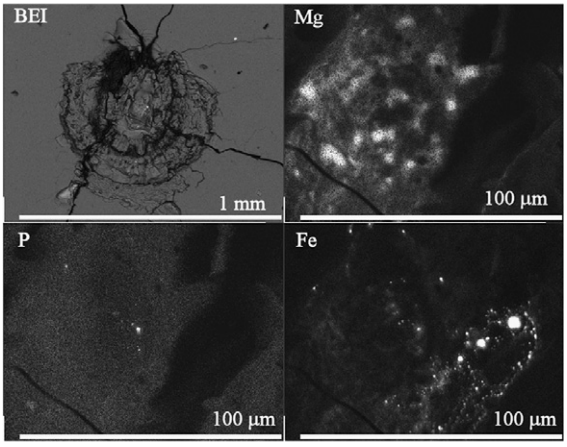

Fig. 4. BEI of large oblique crater; and X-ray maps of Mg, P and Fe in melt pit floor, showing polymineralic residue in oblique impact pit (SM-1, s165).

3.1.3. Fe- and S-rich

These are common residues, found in 21 MM impacts from SM-1 and 13 impacts from SM-3B (e.g. Fig. 3c). They form immiscible melt droplets, which are usually low in nickel. They are very similar to laboratory iron monosulfide impact residues and are probably derived from pyrrhotite or troilite, as widely reported in IDPs and chondritic meteorites (e.g. Noguchi et al., 2002), and recently shown to be present in significant quantities in Antarctic micrometeorites (Duprat et al., 2005).

3.1.4. Iron–nickel metal

These are very distinctive immiscible droplets, visible in BE images due to their high backscatter coefficient (Figs. 5 and 6). Their size varies from 10 nm to 5 μm scale. They were found in three features from SM-1 and 1 from SM-3B. Analyses show a narrow range of composition with Fe:Ni ratio typical of meteoritic kamacite metal (Fig. 3g). In the oblique crater s165, FIB sectioning of an oblate metal spheroid of 2 μm diameter showed crystallographic ion channelling contrast between relict structural domains at sub-micron scale (Fig. 5).

3.1.5. Ca-rich

These residues occur as particles in the shatter and conchoidal zones of four craters from SM-1 and 1 from SM-3B, in each case they are associated with mafic silicate residue in the melt pit (Fig. 7). The residues are probably calcium carbonate, and we have observed similar intact but melt-associated particles from laboratory impacts. The emplacement mechanism and their restriction to the brittle-fractured zones of the crater remain enigmatic.

3.1.6. Mg, Cr, Fe and O-rich

A single tiny residue was found in one crater from SM-1 (s165, Figs. 3 and 4f) in which crater it is associated with Fe–Ni metal, Fe–sulfide, Fe–Ni phosphide and Mg-silicate residues. The residue composition is strongly reminiscent of an oxide phase, probably a chromium-bearing member of the magnesioferrite spinel series.

3.1.7. Fe-, Ni- and P-rich

Three small particles of this composition were found in a single crater (s165) from SM-1. Their spectrum is very similar to that of the meteoritic phosphide schreibersite (Fig. 3e).

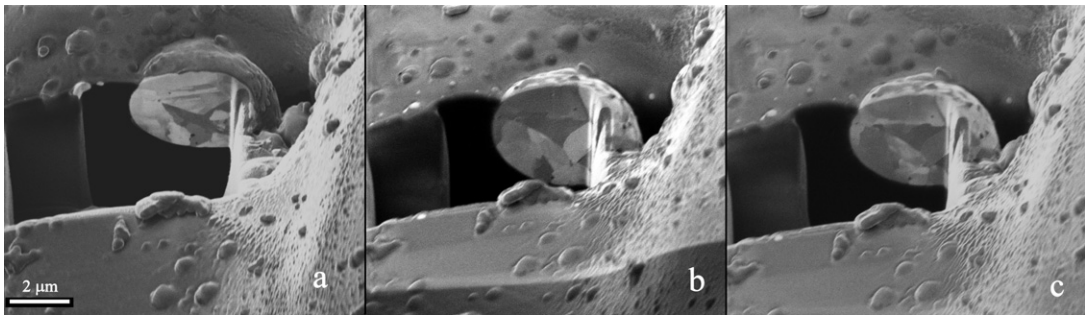

Fig. 5. FIB cross-section and ion images of metal droplet, scale bar 2 μm. (a) at 35 degrees tilt, shows a thin covering of the metal droplet by glass melt (dark grey) before its removal by renewed surface milling, also note the fine scale crystallographic texture in metal, highlighted by ion channelling at 52 degrees tilt (b) and 45 degrees tilt (c).

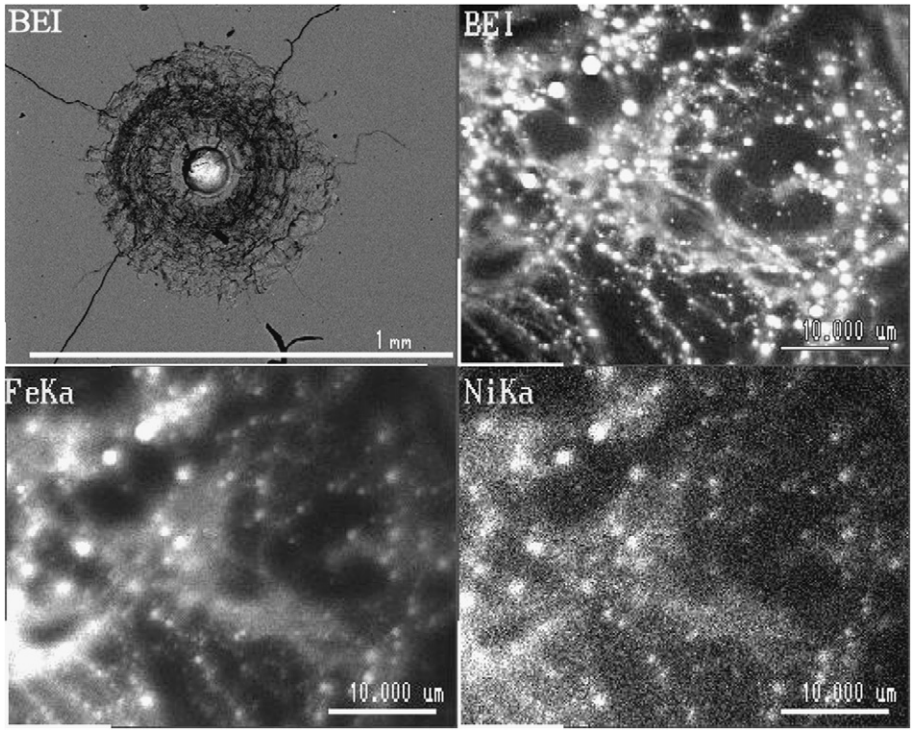

Fig. 6. SM-1 crater s177. BE images at top left shows entire crater, top right shows detail of metal droplets on melt pit floor. X-ray maps show Fe and Ni in abundant metal droplets on the crater floor.

3.1.8. Mg- and S-rich

Small particles rich in magnesium and sulphur were found as loose grains in two craters on the same solar cell from SM-3B. Their X-ray spectrum closely resembles that of the sulfate mineral epsomite.

3.1.9. Al- and Si-rich

These enigmatic aluminosilicate residues, that may represent altered feldspar or mesostasis glass impactors, were found in two craters, one in each of SM-1 and SM-3B (e.g. Fig. 3h).

3.2. How large were the impacting particles?

The size distribution of those measured impact features on the 47 solar cells that can be attributed to micrometeoroid origin is shown in Figs. 8 and 9, spanning a range of 3 orders of magnitude, from 5 μm to 5 mm D_{co}.

The style and scale of impact damage upon solar cell glass is influenced by the relative size of projectile and thickness of individual solar cell layers, as well as by particle velocity and composition. Comparison with other space exposed surfaces, laboratory simulations and computer models of perpendicular impacts on the complex laminated structure of solar cells together have permitted delimitation of a 'damage equation', relating the size of an impacting micrometeoroid and the resulting impact feature dimensions for a given velocity (Grün et al., 1985; Drolshagen et al., 1997; Taylor et al., 1997, 1999). Where impact features include a well-defined melt-pit; radially shattered; conchoidal detachment (spallation); and concentric

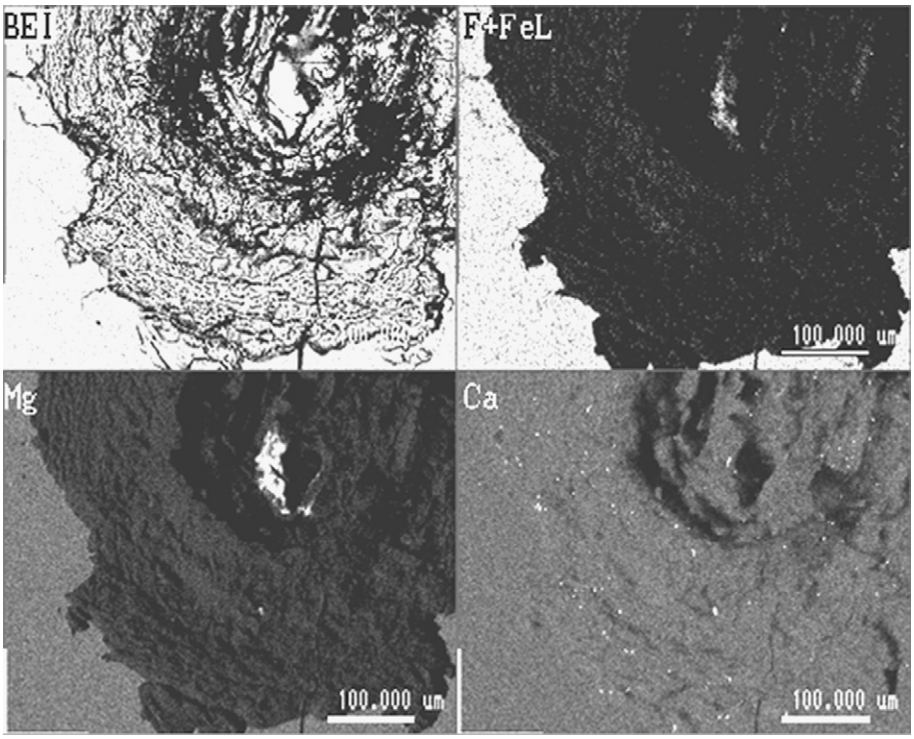

Fig. 7. BEI and X-ray maps for Fe (Fe Lα with F Kα), Mg and Ca, showing mafic silicate residue in the central melt pit and abundant Ca-rich particles on the surface of the conchoidal detachment zone.

fracture zones (Herbert and McDonnell, 1997), it is possible to apply an experimentally determined ratio of spallation zone diameter (D_{co}) to particle diameter (D_p). The relationship has been calibrated by laboratory light gas gun shots between 1 and 7 km s^{-1}, velocities substantially lower than encountered in LEO. Due to uncertainty in the wide range of possible impact velocities for micrometeoroids encountered in LEO, it is difficult to give precise figures for the particle sizes responsible for specific individual features on the HST solar cells. Extrapolation to the velocity range employed by convention for micrometeoroid impacts on spacecraft in LEO (ca. 20 km s^{-1} suggested by Taylor (1995) and employed by Herbert et al. (2001)) yields a D_{co} to D_p ratio that varies from less than 4:1 to as much as 18:1, dependant upon projectile size (and density). According to this calibration, a typical circular crater of D_{co} 1000 μm, bearing iron sulphide and hydrous mafic-silicate residue in a melt pit (e.g. the crater of Fig. 11), could be formed by a micrometeoroid of approximately 50 μm diameter, impacting at a velocity just over 20 km s^{-1}. For features of larger diameter, a different style of damage occurs with penetration through the entire cell thickness, and D_{co} no longer increases so rapidly as a function of the particle diameter. Instead, the diameter of the full-thickness penetration hole may become a simpler proxy for the particle dimensions. The calibration for the smallest features (less than 20 μm D_{co}), suggests the D_{co} to D_p ratio is substantially less than 10:1, perhaps lower than 4:1. If the conventional velocity regime is accepted, it can be seen that there were numerous impacts by particles of between 1 and 10 μm (e.g. over 600 per m^2 per year for SM-3B), with residue being preserved from particles as small as 1.3 μm (Fig. 10). There were few impacts by grains exceeding 100 μm in diameter (e.g. less than 20 per m^2 per year for SM-1), although these account for the vast majority of the mass delivery in Fig. 10. For micrometeoroids of less than 10 μm diameter, there is good agreement between our data and the flux of micrometeoroids at 1 AU as defined by Grün et al. (1985), rescaled for gravitational focus and Earth shielding. For particles larger than 10 μm diameter, our measured flux appears to be substantially greater, but this part of our curve is based upon a very small number of impacts, and errors may be substantial due to the limited number of cells reported in this study (especially when compared to the larger flux data set and huge area-time product of Moussi et al. (2005)). However, the flux of Fig. 10 is based upon very well characterised impacts, and certainly does not include features originating from impact on the rear side of the solar array, a problem discussed by Moussi et al. (2005) but only relevant for impact features with full thickness penetration, exceeding 2 mm D_{co}. A more likely explanation for the high flux can be seen in the work of Sullivan and McDonnell (1992), who demonstrated the importance of facing direction in the interpretation of micrometeoroid flux upon spacecraft surfaces. McBride et al. (1999), in their comparison of measurements between the European Retrievable Carrier (EuReCa) spacecraft

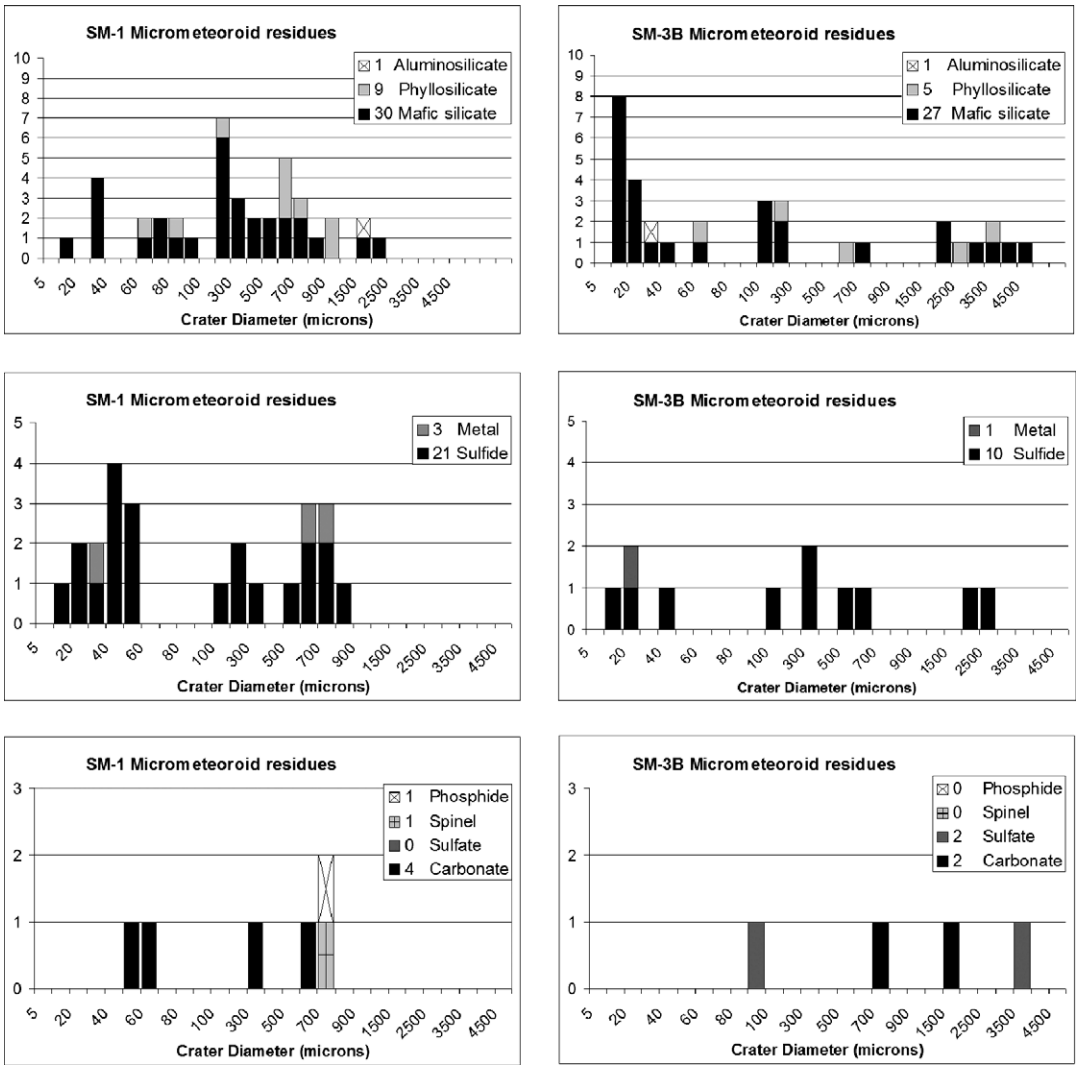

Fig. 8. HST micrometeoroid impact residues. Numbers and sizes of craters containing different residue types. Note changes on the scale for histogram size bin maxima: <5, <20 then bins of 10 μm up to 100 μm, bins of 100 μm to <1000 μm, finally bins of 500 μm to <5000 μm.

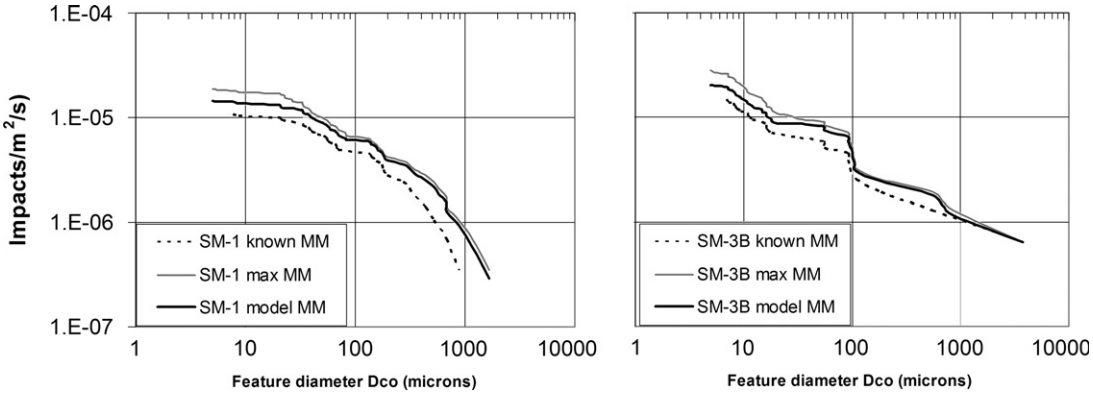

Fig. 9. Cumulative flux plots for the number of micrometeoroid impacts plotted against impact feature size (diameter of conchoidal detachment, D_{co}), based upon analysis of residues in all craters found on randomly selected cells from SM-1 (42 cells) and SM-3B (6 cells). Minimum flux (based upon positive identification of micrometeoroid residue) in thin line, maximum flux (all unresolved impacts assumed to be micrometeoroid) in dashed thin line. The modelled flux (the minimum with addition of unresolved impacts allocated by proportion of determined space debris and micrometeoroid impacts in this size interval) is shown in the bold line. Logarithmic scale on both axes.

and the 'space-facing' end of LDEF, were able to explain the greater number of micrometeoroids on EuReca as a function of the anisotropy of collection, due to a heliocentric facing direction of the solar cells. The sun-facing aspect of the HST solar cell glass surfaces, as surveyed in our work, should generate a similar flux enhancement,

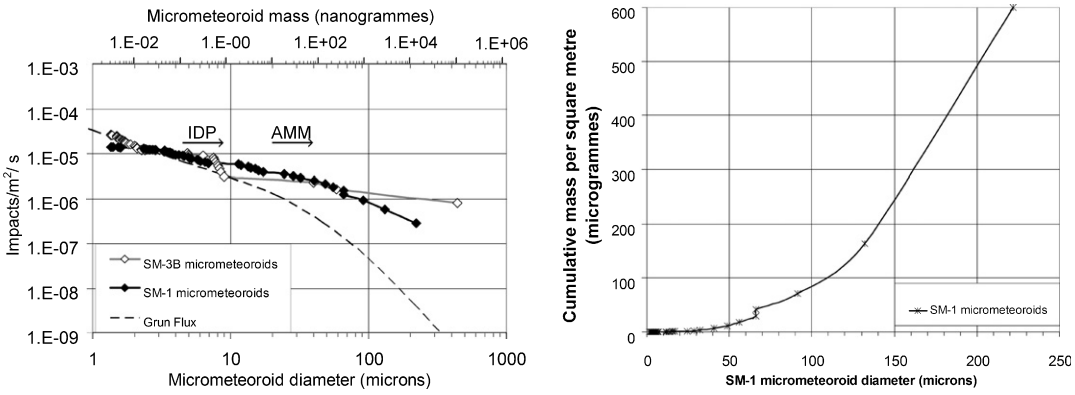

Fig. 10. (Left) Cumulative flux plot for the number of micrometeoroid impacts plotted against particle size (velocity model 20 km s^{-1}), based upon analysis of residues in all craters found on randomly selected cells from SM-1 (42 cells) and SM-3B (6 cells). Logarithmic scale on both axes. SM-1 data shown as open diamonds, SM-3B shown as solid diamonds. The Grün et al. (1985) flux is included (dashed), scaled for Earth shielding and gravitational focusing. Note good agreement below 10 μm particle size, but apparently increased flux relative to Grün et al. (1985) at larger sizes, probably due to an enhanced anisotropic collection of micrometeoroids on the sun-facing solar cell glass of HST, compared to the isotropic sampling of Grün et al. Typical minimum sizes for stratospheric interplanetary dust particles (IDP) and Antarctic micrometeorites (AMM) are shown for comparison. (Right) Cumulative micrometeoroid mass per square metre during the interval from HST launch to SM-1(3.6 years) revealing dominance by a few large particles. Linear scale on both axes.

sufficient to reconcile our data to those of Grün et al. (1985).

Dyrud et al. (2004) suggest that a more appropriate velocity for meteors might be 55–60 km s^1. As their inferred meteor mass range (10^{-11}–10^{-4} g) covers the probable micrometeoroid size range responsible for larger HST impact features, it may be appropriate to modify the particle sizes derived from the damage equation. Herbert et al. (2001) have shown impact feature diameter to be proportional to particle velocity to a power of 0.66, a similar relationship to that for metal crater diameter as described by Humes (1991). Upon this basis we determine that velocity models of 55 km s^{-1} and 70 km s^{-1} would yield smaller inferred particle sizes. If one chooses a 55 km s^{-1} or 70 km s^{-1} model, all the particle sizes across the *X*-axis should be shifted to the left (i.e. to smaller sizes) by multiplication with a factor of 0.51 or 0.44, respectively. This would suggest that the smallest particles are less than 1 μm in diameter, or if a cometary maximum velocity (e.g. 70 km s^{-1}) is chosen as more appropriate for the smallest particles, perhaps as small as 600 nm. Rather than entire IDPs as collected from the stratosphere, these very small individual particles are comparable in size to the sub micron silicates of chondritic aggregate IDPs (Zolensky and Barrett, 1994), and the clumped crystallites forming the granular or polyphase units of Rietmeijer (1998). The grains fall neatly within the mass range for Halley cometary dust as investigated by the Giotto impact detectors (McDonnell et al., 1987), and the particle mass range determined in the vicinity of comet P/Wild2 by the Dust Flux Monitor Instrument aboard the Stardust spacecraft (Tuzzolino et al., 2004). The flux and residue chemistry for even smaller, sub-micron, impact features on HST solar cells has not yet been determined.

3.3. How much residue is preserved?

In most impact features, residue can be found in the hemispherical central melt pit (Figs. 6, 7, 11–13). Trenched sections cut with the FIB (Fig. 11 a and b) revealed residue within a thin layer, approximately 2.5 μm thick, lining approximately 25% of the melt pit interior. Assuming an original spherical morphology for this layer prior to spallation of the overlying glass and loss of the upper half of the melt shell (Fig. 11c and d), the volume of the residue-bearing layer was calculated for the SM-1 crater s322amajor1 (D_{co} of 1104 μm, Fig. 11), by measurement of the diameter of the melt pit inner boundary (Fig. 12). The residue-bearing layer was thus a sub-spherical shell of 205 μm internal diameter and 2.5 μm thickness, whose volume was calculated by subtraction of the outer and inner sphere volumes: $(4/3 * \pi * (102.5 + 2.5)^3) - (4/3 * \pi * (102.5)^3)$. Backscattered electron images and X-ray maps of FIB trench sections showed that approximately 25% of the 2.5 μm layer contained detectable residue mixed with melted solar cell glass. The residue content within the mixture was measured from the mean of two calculations for impactor/glass mixing, using known Mg, K and Zn contents of the cover glass, and analyses of the glass and mixed residue exposed in the trench of Fig. 11. The calculated glass proportion was 70% by weight, and with a mean density estimated at 2.5 g cm^{-3}. Projectile proportion was 30% by weight of the mixture. Based upon interpretation of the projectile composition from the ED spectra as a mixture of tochilinitic serpentine/smectite and iron sulfide, a mean micrometeoroid density of 3.7 g cm^{-3} was assumed. Thus 20% of the melt by volume was residue, with a mass of 120 ng in the full spherical shell (before spallation of the upper hemisphere), and perhaps as much as 50 ng of residue is

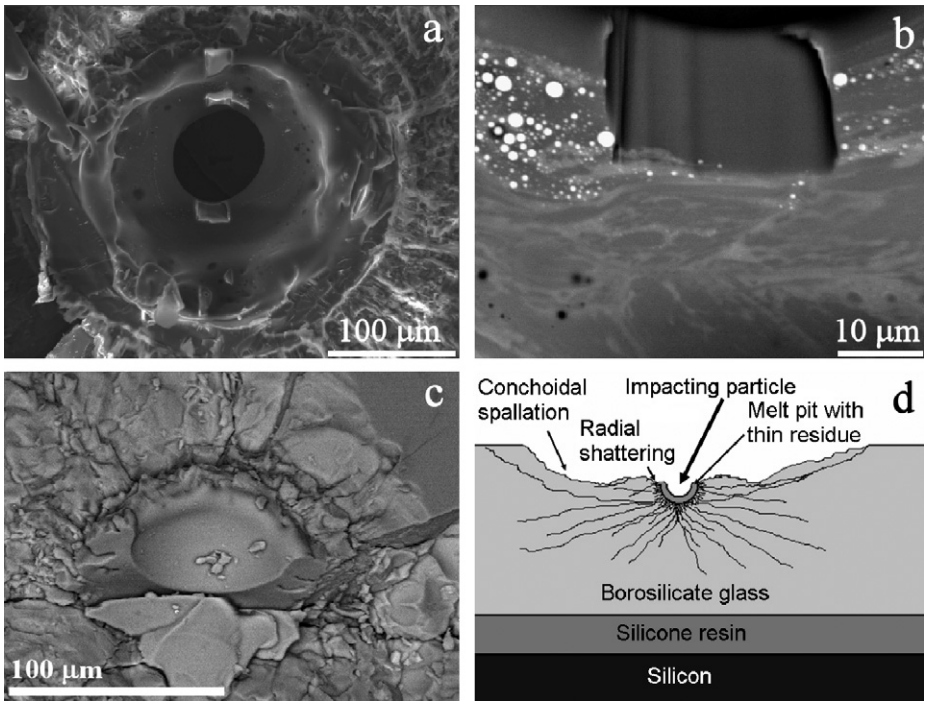

Fig. 11. (a) BEI of melt pit in impact crater s322a1 from SM-1; (b) BEI of trench cut through residue and glass melt, showing about 2.5 μm thickness of Mg-, Fe-, S- and Ni-bearing silicate residue (mid grey), with bright droplets of iron sulfide; (c) BEI of a micrometeoroid impact feature. This oblique view of the partially broken central melt pit shows a hemispherical bowl shape; (d) diagrammatic vertical section through an impact feature on HST solar cell glass, showing the relationship between the hemispherical remnant of the melt pit, the shatter and conchoidal zones. Residue is usually found in a thin layer on the surface of the melt pit.

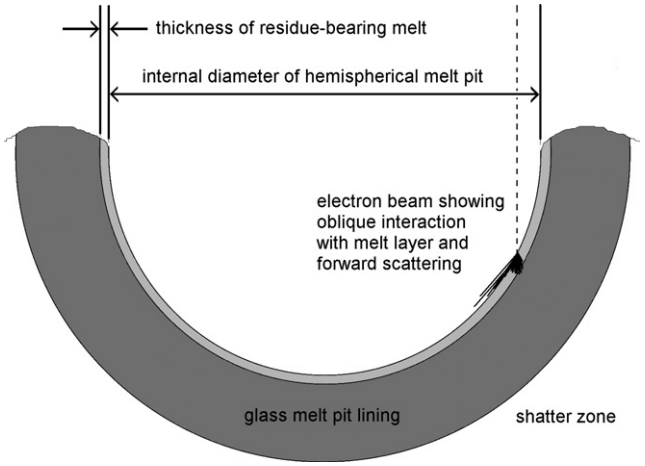

Fig. 12. Diagram of a vertical cross section through a melt pit, showing the dimensions used for calculation of the total volume of residue-bearing melt. The incident electron beam is also shown, to demonstrate the broad and shallow area of X-ray emission on the melt-pit wall, enabling easy recognition of the location of residue.

retained in the remaining melt pit. This is approximately 10% of the probable original particle mass (circa 500 ng) for a 65 μm diameter micrometeoroid of this composition, as inferred responsible for the crater by reference to the damage equation of Herbert et al. (2001), with an appropriate density scaling exponent of 0.44 and velocity of 21.4 km s^{-1}. If a higher velocity model is used for the particle size interpretation, retained percentage appears still higher (75% for the same impact by a smaller particle at 55 km s^{-1}). In some impact features the distribution of residue is more complex, particularly in shallow, elongate and oblique craters where abundant residue is visible (e.g. Fig. 4). Although a similar residue depth distribution is seen within FIB trenches of the melt in oblique craters, the quantity and surviving proportion of residue is much more difficult to calculate, due to the very complex melt pit shape and major uncertainties in the particle size calibration for oblique impacts at an unknown (but probably low) angle of incidence. Nevertheless, such craters do clearly preserve unusually large amounts of residue.

4. Interpretation of particle origins

Several aspects of the residue preservation need to be taken into account before the apparent compositional assemblages can be compared to known extraterrestrial samples that have not undergone hypervelocity impact. Impact of a micrometeoroid upon a solar cell causes violent, albeit very short-lived (nanosecond to microsecond) processing of the projectile, with rapid quenching of a mixture of melted/condensed cover glass and encapsulation of fine droplets derived from the particle. Despite such disruption of particles, each leaves an impact feature, usually with diagnostic residue (ca. 75%). Our work suggests that there is little particle size selection bias in the HST features, in

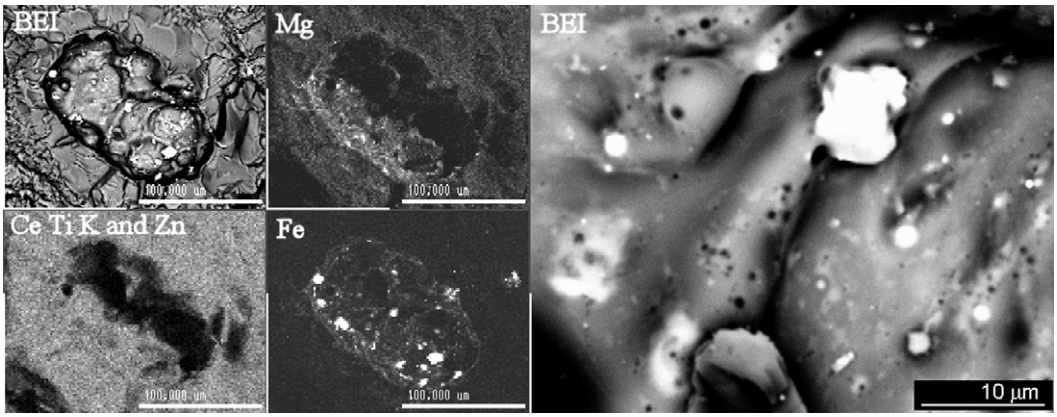

Fig. 13. Light gas gun shot of particle of CI chondrite Orgeuil into solar cell glass. Left hand images are BEI and X-ray maps of Orgeuil residue in pit. At right, BEI shows vesicular residue and discrete iron oxide grains (bright).

contrast to loss of the record of smaller and higher velocity particles due to total evaporation or stripping of reactive components during prolonged melting and oxidation (seconds) in atmospheric entry of many micrometeorites and stratospheric particles. Similarly there is no potential for adsorption of reactive volatile contaminants from the atmosphere, or post-fall alteration in ice or liquid water. We do, however, have very limited knowledge of the characteristics of solar cell impact features and residues from impacts by organic materials and ices.

Light gas gun shots show that relatively volatile elements such as sodium and potassium can be mobilised during the impact process leading to local depletion, or occasionally enrichment, of these elements. Their apparent absence from the HST residues might therefore not be due to an absence of alkali-enriched glass (such as is found in chondrule mesostasis) or feldspar grains, so much as a preservation bias. However, the paucity of calcium-enriched aluminosilicate residues (2/106) is significant. Calcium is much more refractory, and should be expected to be retained and enriched relative to other elements, rather than depleted by volatilisation. The relatively low calcium content of the HST cover glass should also provide an ideal substrate upon which to recognise the presence of Ca-bearing melt. In light gas gun shots, Ca- and Na-rich plagioclase feldspars and glasses leave residues that are easily recognised. The rarity of residue rich in Ca and Al also suggests that there is little contribution from the refractory mineral inclusions such as the hibonite and gehlenite bearing particles reported by Greshake et al. (1996), or the high-Ca clinopyroxene found in abundance within the matrix of CV carbonaceous chondrites, such as Allende. It therefore seems that HST impacts do again reflect the substantial difference in the composition and origin of most smaller meteoroids (micron to 10 micron-scale) when compared to coarser (centimetre to metre-scale) materials at 1 AU, as has been indicated by studies of IDPs, summarised by Rietmeijer (1998) and micrometeorites (Kurat et al., 1994; Beckerling and Bischoff, 1995). This view is reinforced by suggestion that the calcium and aluminium bearing 'low-Ni' IDPs of Flynn and Sutton (1990) may be terrestrial volcanic particles rather than extraterrestrial (Rietmeijer, 1998).

Unfortunately, the wispy mafic silicate residues so frequently encountered in HST impacts do not preserve many diagnostic characteristics that allow close comparison to either a particular micrometeorite group, or to IDP crystalline phase or glass. The ratio of divalent ions to silicon cannot be determined in most residues, due to the overwhelming silicon content of the solar cell glass. This prevents calculation of the olivine to pyroxene ratio within most of the particle population, thereby removing a potentially valuable diagnostic criterion of origin, and does not permit easy comparison to the chondritic signature seen in many IDPs (e.g. Brownlee et al., 1976) or the Mg/Si and Al/Si ratios so useful in IDP classification (Fraundorf et al., 1982). The lack of preserved internal structures and phase relationships also hinders comparison to documented IDP and micrometeorite textures. However, the occasional presence of vesicular Fe- and Mg-bearing melt does indicate that volatile rich, probably hydrous, minerals were present among the particles. Similar bubble-rich textures were seen in a few residues from our laboratory shots of the pyroxene enstatite, containing small quantities of the hydrated layer silicate talc. Enrichment of sulfur and nickel within the vesicular mafic HST residues strongly suggests that these may represent a fine-grained phyllosilicate assemblage such as those reported from IDPs (Schramm et al., 1989; Zolensky and Lindstrom, 1992), hydrated micrometeorites (Kurat et al., 1994; Genge et al., 1997; Noguchi et al., 2002), C2 microclasts in howardites (Gounelle et al., 2003) or carbonaceous chondrites of the CI and CM groups (e.g. Genge et al., 1997; Noguchi et al., 2002). It is not possible to use Mg and Fe to Si ratios to determine whether saponite or serpentine was present in the hydrous particles impacting on HST solar cells, although the presence of diffuse nickel and sulfur in some of the vesicular residues may suggest a close relationship

with the tochilinite–serpentine interlayer materials found in CM chondrites, the fossil CM micrometeorites of Gounelle et al. (2003), and some IDPs (Bradley and Brownlee, 1991). Light gas gun shots of powder from the CI type 1 carbonaceous chondrite Orgeuil and the CM type 2 Murchison demonstrate that their fine matrix does indeed generate a vesicular melt of this type (Figs. 3 and 13b). It is interesting that the number of HST residues suggests a higher proportion of volatile-rich silicate grains (14 out of 71 mafic silicate bearing residues) than Nakamura et al., 2001 report from Antarctic micrometeorites, although Genge et al. (1997) imply that phyllosilicates must be more common in the micrometeoroid precursor population as the textures of their vesicular unmelted micrometeorites (VMM) were derived from phyllosilicate-rich precursors, a view supported by the observations of Noguchi et al. (2002) and the experiments of Toppani et al. (2001).

The abundant and easily recognised magnetite grains seen in CI meteorites, which are so obvious in laboratory impact residues from Orgeuil (Fig. 13), are not found in our LEO craters, and Genge et al. (1997) also note the paucity of this mineral in their VMM particles, although it is reported as framboids in phyllosilicate-rich micrometeorites by Noguchi et al. (2002), and in the CR type microclasts in howardites by Gounelle et al. (2003). Secondary magnetite, occurring as a thin coating on silicate grains in chondritic aggregate IDPs has been attributed to atmospheric entry effects (e.g. Fraundorf, 1981), but should be absent from such particles impacting on a spacecraft surface at 600 km altitude. Noguchi et al. (2002) also suggest that magnesiowustite and magnetite may be generated as breakdown products of ferroan carbonates during atmospheric heating. Magnetite has been reported from solar wind irradiation of metal grains within IDPs (Bradley, 1994) although residues from particles of this extremely fine grain size (10 s of nm) may be difficult to recognise in analytical SEM studies.

The presence of sulfate and carbonate residues in larger (mm scale) impacts on HST cells is also noteworthy. These minerals, well known from CM chondrites, may support an origin from an asteroidal source, with deposition requiring a hydrological system such as that suggested by Wilson et al. (1999). The survival of relatively delicate and soluble sulfates and carbonates in HST impact residues is in contrast to their absence from most Antarctic micrometeorites, from which they are have probably been lost due to thermal decomposition (Noguchi et al., 2002), or removed by aqueous leaching, as reported by Kurat et al. (1994). Carbonates have been reported in howardite microclasts (Gounelle et al., 2003).

HST residues from impacts by particles of greater than 10 μm diameter often contain distinct iron sulfide droplets, yet sulfide has been reported as rare in Antarctic micrometeorites (e.g. Genge et al., 1997). Possible removal of sulfide during atmospheric transit has been discussed by Genge and Grady (1998), but recent work by Duprat et al. (2005) has shown that careful separation of smaller Antarctic micrometeorites can yield substantial numbers of sulfide-bearing grains. The HST iron sulfide residues resemble compositions found throughout ordinary chondrites, CM and CI carbonaceous chondrites (although less common in CV and CK) and also found in mesosiderites. The iron–nickel metal is very similar to the composition of the kamacite phase known from IDPs, iron and stony iron meteorites, and the finely structured metal found in ordinary chondrite meteorites.

The assemblage of olivine, finely crystalline iron-nickel metal, iron sulfides, iron–nickel phosphides and chromium-bearing oxides within a single crater (Fig. 6) is strongly reminiscent of pallasite stony-iron meteorites such as Brahin. However, pallasites show coarse (millimetre to centimetre) grain size, and it seems unlikely that a micrometeoroid smaller than a millimetre would contain the examples of each diagnostic mineral. The magnesium-, iron- and chromium-bearing spinel composition is certainly unlike that of refractory inclusion spinels in carbonaceous chondrites (almost end-member unequilibrated magnesian aluminous spinel sensu strictu, subsequently altered by iron enrichment), although similar compositions do occur in ordinary chondrites. Low magnesium, chromian magnetites also occur widely in CV and CK chondrites (Greenwood et al., 2004), where they may be found within olivine-bearing chondrules, associated with iron–nickel metal, minor phosphide and sulphide. The oblique impact in Fig. 6 may thus represent impact by a chondrule fragment.

5. Conclusions and future work

LEO impact craters on solar cells yield abundant residues, from which micrometeoroid mineral precursors can be interpreted. As well as making measurement of micrometeoroid flux, we are now able to ascribe compositional information to impacting particles across a size range from micrometre to hundreds of micrometres diameter. A substantial proportion of the micrometeoroid may be preserved, especially in oblique craters. It is not yet possible to determine the precise source of the abundant mafic silicate grain impactors, but there is good evidence for some impacts by hydrous sheet silicate phases similar to those seen in type 1 and 2 carbonaceous chondrite meteorites, phyllosilicate-rich micrometeorites and interplanetary dust particles. There is a notable anomaly in the lack of calcium-bearing aluminosilicates residues, implying that chondrule mesostasis glass, matrix plagioclase and the refractory inclusions of carbonaceous chondrites are not well represented in the residue population.

Our initial results suggest that focused ion-beam cross-sections of shocked but compositionally discrete mineral residues can be used for electron microprobe analysis, and have promise for electron diffraction and micro-source X-ray diffraction study of shock state, as well as isotopic analysis. Ultrathin sections of finer immiscible droplet residues may also be suitable for analytical trans-

mission electron microscopy, enabling distinction of olivine and pyroxene residues in a greater number of craters. Identification of the diverse mineral assemblages to be found in residue-rich larger oblique impacts, of millimetre scale, may provide a direct link to the petrology of micrometeorites.

Acknowledgements

Study of SM-1 was funded by ESA Contract No. 13308/98/NL/MV, and study of SM-3B craters by UniSpaceKent ESA Contract No. 16283/02/GD/ESTEC. Giles Graham acknowledges PPARC Case studentship and post-doctoral funding, and his recent work was under the auspices of the U.S. Department of Energy, National Nuclear Security Administration by the University of California, Lawrence Livermore National Laboratory under Contract No. W-7405-Eng-48. We thank Dave Wallis and Mike Cole for performing Light Gas Gun shots at the University of Kent (Canterbury) and Peter Lord for FIB cross-sectioning and imaging. We are particularly grateful to the crews of STS-61 and STS-109 and all the supporting mission teams for their dedication and hard work in retrieving the solar arrays. FIB analysis was performed at Imperial College, electron microscopy at Oxford Brookes University and in the Natural History Museum, London. The very helpful comments of the reviewing referees are gratefully acknowledged.

References

Alexander, C.M., Love, S.G. Atmospheric entry heating of micrometeorites revised: higher temperatures and potential biases (abstract). LPSC, XXXII, #1935, 2001.

Beckerling, A., Bischoff, A. Occurrence and composition of relict minerals in micrometeorites from Greenland and Antarctica – implications for their origins. Planet. Space Sci. 43, 439–449, 1995.

Bernhard, R.P., Durin, C., Zolensky, M.E. Scanning Electron Microscope/Energy Dispersive X-ray analysis of impact residues in LDEF tray clamps, in: Levine, A.S. (Ed.), LDEF-69 months in space, Part 2. NASA Conference publication 3194, National Aeronautics and Space Administration, Washington, D.C., USA, pp. 541–549, 1994.

Bradley, J.P. Chemically anomalous, pre-accretionally irradiated grains in interplanetary dust from comets. Science 265, 925–929, 1994.

Bradley, J.P. Interplanetary dust particles, in: Davis, A.M., Holland, H.D., Turekian, K.K. (Eds.), Treatise on Geochemistry, vol. 1. Elsevier, Amsterdam, pp. 689–711, 2004.

Bradley, J.P., Brownlee, D.E. An interplanetary dust particle linked directly to type CM chondrites and an asteroidal origin. Science 251, 549–552, 1991.

Brownlee, D.E. Cosmic Dust: collection and research. Ann. Rev. Earth Plan. Sci. 13, 147–173, 1985.

Brownlee, D.E., Tomandl, D.A., Hodge, P.W. Extraterrestrial particles in the stratosphere, in: Elsasser, H., Fechtig, H. (Eds.), Interplanetary Dust and the Zodiacal Light. Springer-Verlag, New York, pp. 279–284, 1976.

Burchell, M.J., Cole, M.J., McDonnell, J.A.M., Zarnecki, J.C. Hypervelocity impact studies using the 2 MV Van de Graaff accelerator and two-stage light gas gun of the University of Kent at Canterbury. Meas. Sci. Technol. 10, 41–50, 1999.

Drolshagen, G., Carey, W.C., McDonnell, J.A.M., Stevenson, T.J., Mandeville, J.-C., Berthoud, L. HST solar array impact survey: revised damage laws and residue analysis. Adv. Space Res. 19, 239–251, 1997.

Duprat, J., Engrand, C., Maurette, M., Gounelle, M., Kurat, G., Leroux, H. Friable micrometeorites from Central Antarctica snow (abstract), LPSC, XXXVI, #1678, 2005.

Dyrud, L.P., Denney, K., Close, S., Oppenheim, M., Chau, J., Ray, L. Meteor velocity determination with plasma physics. Atmos. Chem. Phys. 4, 817–824, 2004.

Flynn, G.J., Sutton, S.R. Synchrotron X-ray fluorescence analyses of stratospheric cosmic dust: new results for chondritic and low nickel particles. Proc. Lunar Planet. Sci Conf. 20, 335–342, 1990.

Fraundorf, P. Interplanetary dust in the transmission electron microscope: diverse materials from the early solar system. Geochim. Cosmochim. Acta 45, 915–943, 1981.

Fraundorf, P., McKeegan, K.K.D., Sandford, S.A., Swan, P., Walker, R.M. An inventory of particles from stratospheric collectors: Extraterrestrial and otherwise. J. Geophys. Res. 87, A403–A408, 1982.

Genge, M.J., Grady, M.M. Melted micrometeorites from Antarctic ice with evidence for the separation of immiscible Fe–Ni–S liquids during entry heating. Meteorit. Planet. Sci. 33, 425–434, 1998.

Genge, M.J., Grady, M.M., Hutchison, R. The textures and compositions of fine-grained Antarctic micrometeorites: implications for comparisons with meteorites. Geochim. Cosmochim. Acta 61, 5149–5162, 1997.

Graham, G.A., Chater, R.J., McPhail, D.S., Kearsley, A.T., Lee, M.R., Kettle, S., Wright, I.P. In situ sectioning and analysis of cosmic dust using Focused Ion Beam microscopy (Abstract). Meteorit. Planet. Sci. 37 (suppl.), A56, 2002.

Graham, G.A., Kearsley, A.T., Grady, M.M., Wright, I.P., Griffiths, A.D., McDonnell, J.A.M. The collection of micrometeoroid remnants from low earth orbit. Adv. Space Res. 25 (2), 207–303, 2000.

Graham, G.A., Kearsley, A.T., Grady, M.M., Wright, I.P., Herbert, M.K., McDonnell, J.A.M. Natural and Simulated Hypervelocity impacts into solar cells. Int. J. Impact Eng. 23, 319–330, 1999.

Graham, G.A., Kearsley, A.T., Wright, I.P., Grady, M.M., Drolshagen, G., McBride, N.M., Green, S.F., Burchell, M.J., Yano, H., Elliott, R. Analysis of impact residues on spacecraft surfaces: possibilities and problems, in: Sawaya-Lacoste, H. (Ed.), Proceedings of the 3rd European Conference on Space Debris. ESA Publications Division, ESTEC, Noordwijk, The Netherlands, ESA Spec. Pub. 473, pp. 197–203, 2001a.

Graham, G.A., McBride, N., Kearsley, A.T., Drolshagen, G., Green, S.F., McDonnell, J.A.M., Grady, M.M., Wright, I.P. The chemistry of micrometeoroid and space debris remnants captured on Hubble Space Telescope Solar Cells. Int. J. Impact Eng. 26, 263–274, 2001b.

Greenwood, R.C., Franchi, I.A., Kearsley, A.T., Alard, O. The relationship between CK and CVchondrites: a single parent body source? (abstract). LPSC XXXV, #1664, 2004.

Greshake, A., Hoppe, P., Bischoff, A. Mineralogy, chemistry and oxygen isotopes of refractory inclusions from stratospheric interplanetary dust particles and micrometeorites. Meteorit. Planet. Sci. 31, 739–748, 1996.

Gounelle, M., Zolensky, M.E., Liou, J.-C., Bland, P.A., Alard, O. Mineralogy of carbonaceous chondritic microclasts in howardites: Identification of C2 fossil micrometeorites. Geochim. Cosmochim. Acta 67, 507–527, 2003.

Grün, E., Zook, H.A., Fechtig, H., Giese, R.H. Collisional balance of the meteoritic complex. Icarus 62, 244–272, 1985.

Herbert, M.K., McDonnell, J.A.M. Morphological classification of impacts on the EuReCa and Hubble Space Telescope solar arrays, in: Kaldeich-Schürmann, B., Harris, B. (Eds.), Proceedings of the 2nd European Conference on Space Debris. ESA Publications Division, ESTEC, Noordwijk, The Netherlands, ESA Spec. Pub. 393, pp. 169–178, 1997.

Herbert, M.K., Mandeville, J.-C., Taylor, E.A., McDonnell, J.A.M. Analogies and differences between quasistatic indentation and hypervelocity impact morphologies on thin solar cells. Int. J. Impact Eng. 26, 321–331, 2001.

Humes, D.H. Large craters on the meteoroid and space debris impact experiment, in: Levine, A.S. (Ed.), LDEF-69 months in space. NASA

Conference publication 3134, Part 1. National Aeronautics and Space Administration, Washington, D.C., USA, pp. 399–418, 1991.

Hörz, F., Bernhard, R.P., See, T.H., Kessler, D.J. Metallic and oxidized aluminum debris impacting the trailing edge of the Long Duration Exposure Facility (LDEF). Space Debris 2, 51–66, 2002.

Hörz, F., Fechtig, H., Janicke, J., Schneider, E. Morphology and projectile residue in small experimental craters. J. Geophys. Res. 88, 353–363, 1983.

Hörz, F., Zolensky, M.E., Bernhard, R.P., See, T.H., Warren, J.L. Impact Features and Projectile Residues in Aerogel Exposed on Mir. Icarus 147, 559–579, 2000.

Kearsley, A.T., Drolshagen, G., McDonnell, J.A.M., Mandeville, J.-C., Moussi, A. Impacts on Hubble Space Telescope solar arrays: discrimination between natural and man-made particles. Adv. Space Res. 35, 1254–1262, 2005.

Kurat, G., Koeberl, C., Presper, T., Brandstatter, F., Maurette, M. Petrology and Geochemistry of Antarctic micrometeorites. Geochim. Cosmochim. Acta 58, 3879–3904, 1994.

Love, S.G., Brownlee, D.E. A direct measurement of the terrestrial mass accretion rate of cosmic dust. Science 262, 550–553, 1993.

McBride, N., Green, S.F., McDonnell, J.A.M. Meteoroids and small-sized debris in low Earth orbit and at 1 AU: results of recent modelling. Adv. Space Res. 23.1, 73–82, 1999.

McDonnell, J.A.M., Alexander, W.M., Burton, W.M., Bussoletti, E., Evans, G.C., Evans, S.T., Firth, J.G., Grard, R.J., Green, S.F., Grun, E., Hanner, M.S., Hughes, D.W., Igenbergs, E., Kissel, J., Kuczera, H., Lindblad, B.A., Langevin, Y., Mandeville, J.-C., Nappo, S., Pankiewicz, G.S., Perry, C.H., Schwehm, G.H., Sekanina, Z., Stevenson, T.J., Zarnecki, J. The dust distribution within the inner coma of comet P/Halley 1982i: encounter by Giotto's impact detectors. Astron. Astrophys. 187, 719–741, 1987.

McDonnell, J.A.M., Griffiths, S.D. (Eds.), Meteoroid and debris flux and ejecta Models. Summary Report of European Space Agency contract 11887/96/NL/JG. UniSpace Kent, Canterbury, United Kingdom, <http//space-env.esa.int/R_and_D/eureca/Sum_Rpt.pdf/>, 1998.

Moussi, A., Drolshagen, G., McDonnell, J.A.M., Mandeville, J.-C., Kearsley, A.T., Ludwig, H. Hypervelocity impacts on HST solar arrays and the debris population. Adv. Space Res. 35, 1243–1253, 2005.

Nakamura, T., Noguchi, T., Yada, T., Nakamuta, Y., Takaoka, N. Bulk mineralogy of individual micrometeorites determined by X-ray diffraction analysis and transmission electron microscopy. Geochim. Cosmochim. Acta 65, 4385–4397, 2001.

Noguchi, T., Nakamura, T., Nozaki, W. Mineralogy of phyllosilicate-rich micrometeorites and comparison with Tagish Lake and Sayama meteorites. Earth Planet. Sci. Lett. 202, 229–246, 2002.

Peucker-Ehrenbrink, B., Ravizza, G. The effects of sampling artifacts on cosmic dust flux estimates: a reevaluation of nonvolatile tracers (Os, Ir). Geochim. Cosmochim. Acta. 64 (11), 1965–1970, 2000.

Rietmeijer, F.J.M. Interplanetary dust particles, in: Papike, J.J. (Ed.), Planetary Materials Min. Soc. America, Reviews in Mineralogy, 36, Chapter 2, pp. 1–95, 1998.

Schramm, L.S., Brownlee, D.E., Wheelock, M.M. Major element composition of stratospheric micrometeorites. Meteoritics 24, 99–112, 1989.

Sullivan, K., McDonnell, J.A.M. LDEF flux anisotropy: dynamic modelling and flux transformations to define the interplanetary micrometeoroid environment, in: McDonnell, J.A.M. (Ed.), Hypervelocity Impacts in Space. University of Kent, Canterbury, United Kingdom, pp. 126–132, 1992.

Svedhem, H., Drolshagen, G., Grün, E., Grafodatsky, O., Prokopiev, U. New results from in situ measurements of cosmic dust – data from the Gorid experiment. Adv. Space Res. 25 (2), 309–314, 1999.

Taylor, A.D. The Harvard Radio Meteor Project velocity distribution reappraised. Icarus 116, 154–158, 1995.

Taylor, E.A., Kay, L., Shrine, N.R.G. Hypervelocity impact on seminfinite brittle materials: fracture morphology related to projectile diameter. Adv. Space Res. 20, 1437–1440, 1997.

Taylor, S., Lever, J.H., Harvey, R.P. Accretion rate of cosmic spherules measured at the South Pole. Nature 392 (6679), 899–903, 1998.

Taylor, E.A., Shrine, N.R.G., McBride, N., Green, S.F., McDonnell, J.A.M., Drolshagen, G. Impacts on HST and EURECA solar arrays compared with LDEF using a new glass-to-aluminium conversion. Adv. Space Res. 23 (1), 83–87, 1999.

Toppani, A., Libourel, G., Engrand, C., Maurette, M. Experimental simulation of atmospheric entry of meteorites. Meteorit. Planet. Sci. 36, 1377–1396, 2001.

Tuzzolino, A.J., Economou, T.E., Clark, B.C., Tsou, P., Brownlee, D.E., Green, S.F., McDonnell, J.A.M., Colwell, M.T.S.H. Dust measurements in the coma of comet 81P/Wild2 by the Dust Flux Monitor Instrument. Science 304, 1776–1780, 2004.

Wilson, L., Keil, K., Browning, L.B., Krot, A.N., Bourcier, W. Early aqueous alteration, disruption and reprocessing of asteroids. Meteorit. Planet. Sci. 34, 541–557, 1999.

Zolensky, M.E., Lindstrom, D. Mineralogy of 12 large "chondritic" interplanetary dust particles. Proc. Lunar Planet. Sci. Conf. 22, 161–169, 1992.

Zolensky, M.E., Pieters, C., Clark, B., Papike, J. Small is beautiful; analysis of nanogram-sized astromaterials. Meteorit. Planet. Sci. 35, 9–29, 2000.

Zolensky, M.E., Barrett, R. Olivine and pyroxene compositions of chondritic interplanetary dust particles, in: Zolensky, M.E., Wilson, T.L., Rietmeijer, F.J.M., Flynn, G.J. (Eds.), Analysis of Interplanetary Dust. AIP Conference Proceedings. American Institute of Physics, New York, 310, pp. 105–114, 1994.